



## TECHNICAL ADVANCE

# Robotic Assay for Drought (RoAD): an automated phenotyping system for brassinosteroid and drought responses

Lirong Xiang<sup>1,†</sup>, Trevor M. Nolan<sup>2,3,†,‡</sup>, Yin Bao<sup>1,§</sup>, Mitch Elmore<sup>4</sup>, Taylor Tuel<sup>1</sup>, Jingyao Gai<sup>1</sup>, Dylan Shah<sup>1</sup>, Ping Wang<sup>2</sup>, Nicole M. Huser<sup>2</sup>, Ashley M. Hurd<sup>2</sup>, Sean A. McLaughlin<sup>2</sup>, Stephen H. Howell<sup>2,3</sup>, Justin W. Walley<sup>3,4</sup>, Yanhai Yin<sup>2,3,\*</sup>  and Lie Tang<sup>1,3,\*</sup> 

<sup>1</sup>Department of Agricultural and Biosystems Engineering, Iowa State University, Ames, IA 50011, USA,

<sup>2</sup>Department of Genetics, Development and Cell Biology, Iowa State University, Ames, IA 50011, USA,

<sup>3</sup>Plant Sciences Institutes, Iowa State University, Ames, IA 50011, USA, and

<sup>4</sup>Department of Plant Pathology and Microbiology, Iowa State University, Ames, IA 50011, USA

Received 12 June 2020; revised 16 June 2021; accepted 19 June 2021; published online 3 July 2021.

\*For correspondence (e-mail yin@iastate.edu [YY]; lietang@iastate.edu [LT]).

†These authors contributed equally to this work.

‡Present address: Department of Biology, Duke University, Durham, NC, 27708, USA

§Present address: Department of Biosystems Engineering, Auburn University, Auburn, AL, 36849, USA

## SUMMARY

Brassinosteroids (BRs) are a group of plant steroid hormones involved in regulating growth, development, and stress responses. Many components of the BR pathway have previously been identified and characterized. However, BR phenotyping experiments are typically performed in a low-throughput manner, such as on Petri plates. Additionally, the BR pathway affects drought responses, but drought experiments are time consuming and difficult to control. To mitigate these issues and increase throughput, we developed the Robotic Assay for Drought (RoAD) system to perform BR and drought response experiments in soil-grown *Arabidopsis* plants. RoAD is equipped with a robotic arm, a rover, a bench scale, a precisely controlled watering system, an RGB camera, and a laser profilometer. It performs daily weighing, watering, and imaging tasks and is capable of administering BR response assays by watering plants with Propiconazole (PCZ), a BR biosynthesis inhibitor. We developed image processing algorithms for both plant segmentation and phenotypic trait extraction to accurately measure traits including plant area, plant volume, leaf length, and leaf width. We then applied machine learning algorithms that utilize the extracted phenotypic parameters to identify image-derived traits that can distinguish control, drought-treated, and PCZ-treated plants. We carried out PCZ and drought experiments on a set of BR mutants and *Arabidopsis* accessions with altered BR responses. Finally, we extended the RoAD assays to perform BR response assays using PCZ in *Zea mays* (maize) plants. This study establishes an automated and non-invasive robotic imaging system as a tool to accurately measure morphological and growth-related traits of *Arabidopsis* and maize plants in 3D, providing insights into the BR-mediated control of plant growth and stress responses.

**Keywords:** *Arabidopsis thaliana*, Brassinosteroid, drought, leaf segmentation, phenotypic traits, plant growth, 2D and 3D imaging, technical advance.

## INTRODUCTION

Drought, or limited availability of water, looms as one of the most pressing threats to agriculture. As the world's population increases, an important challenge is to engineer plants that withstand stresses such as drought while optimizing their growth (Gupta *et al.*, 2020). To realize this

goal, we need to understand how plant growth and stress responses are balanced. Such dissection requires comprehensive characterization of growth- and drought-related phenotypes along with the underlying signaling pathways that coordinate these responses. One such pathway is activated by a group of plant steroid hormones called

brassinosteroids (BRs) that function as critical regulators of plant growth, development, and drought responses (Nolan *et al.*, 2017a; Nolan *et al.*, 2020).

BRs signal through plasma membrane receptors BRI1 and BAK1 to regulate the activities of BES1 and BZR1 family transcription factors, which control the expression of thousands of genes for various BR responses (Nolan *et al.*, 2020; Sun *et al.*, 2010; Yu *et al.*, 2011). Mutants defective in the BR pathway such as *bri1* are dwarf in stature with reduced stem elongation, shorter and rounder leaves (Li *et al.*, 1996; Szekeres *et al.*, 1996; Clouse *et al.*, 1996), and increased tolerance to stresses such as drought (Nolan *et al.*, 2017a; Nolan *et al.*, 2017b; Northey *et al.*, 2016; Ye *et al.*, 2017). In contrast, gain-of-function mutants in the BR pathway display increased plant growth but often have reduced survival during drought (Nolan *et al.*, 2017a; Ye *et al.*, 2017).

BR phenotyping experiments are typically performed on Petri plates at the seedling stage and/or in a low-throughput manner. Since BRs affect plant growth and development at multiple stages of plant life, it would be helpful to comprehensively measure BR-related phenotypes in a time-dependent manner with an automated system. Additionally, drought experiments have often been conducted by subjecting plants to extreme water deficit conditions that are difficult to control or scale to a large number of genotypes. Several automated drought phenotyping systems have been developed that allow for more mild drought stress scenarios and have provided significant insights into growth regulation under these conditions (Clauw *et al.*, 2015; Dubois and Inzé, 2020; Granier *et al.*, 2006; Skiryecz *et al.*, 2011; Tisné *et al.*, 2013; Van Dooren *et al.*, 2020). Thus, automated phenotyping of BR and drought responses has great potential to further define the interplay between growth and drought responses.

Recently, several image-based phenotyping systems have been established for large-scale and non-destructive phenotyping under controlled environments (Bao *et al.*, 2019b; Fujita *et al.*, 2018; Granier *et al.*, 2006; Skiryecz *et al.*, 2011; Tisné *et al.*, 2013). Various advanced sensor technologies have been successfully integrated into phenotyping systems, including visible RGB imaging (Minervini *et al.*, 2014; Clauw *et al.*, 2015), chlorophyll fluorescence imaging (Rousseau *et al.*, 2013; Yao *et al.*, 2018), thermal imaging (Klem *et al.*, 2017; Zia *et al.*, 2013), and hyperspectral imaging (Behmann *et al.*, 2018; Ge *et al.*, 2016). While both commercial (Neumann *et al.*, 2015; Skiryecz *et al.*, 2011) and custom-built platforms (Apelt *et al.*, 2015; Tisné *et al.*, 2013) have been created, most current systems are limited to 2D imaging and lack the flexibility to administer different types of treatments or compounds. However, 2D methods cannot reflect spatial and temporal information due to plants' architectural complexity (Apelt *et al.*, 2015; Gibbs *et al.*, 2018). Measurements such as plant volume,

plant surface area, and leaf inclination angle are all vital to plant growth monitoring, but cannot be derived from 2D images.

To overcome the inherent limitations of 2D-based approaches, 3D imaging has gained great interest in plant phenotyping. Methodologies for reconstructing 3D models in plant phenotyping platforms can be categorized into passive and active methods (Bernotas *et al.*, 2019). One of the most popular passive methods is multi-view stereo (MVS). An *et al.* (2017) developed an MVS-based system for monitoring a mapping population of 1050 Arabidopsis plants, where 108 digital cameras along with photogrammetric techniques were used to reconstruct 3D shapes. As an alternative to MVS-based imaging, a 3D light-field camera has been utilized to capture high-resolution 3D leaf surfaces of Arabidopsis plants throughout the diel cycle (Apelt *et al.*, 2015). One of the common limitations of the passive approaches is that they require consistent lighting conditions to acquire high-quality images. Therefore, the existing platforms that utilize passive 3D sensors are mostly stationary with fixed camera positions. Active 3D imaging approaches for plant modeling include time-of-flight (ToF) cameras (Hu *et al.*, 2018), laser scanners (Chaudhury *et al.*, 2017), and photometric cameras (Bernotas *et al.*, 2019). A ToF camera provides an economical solution for plant 3D modeling but the resolution is relatively low. Both laser scanners (Kaminuma *et al.*, 2004) and photometric cameras (Bernotas *et al.*, 2019) have been used for Arabidopsis plant phenotyping due to their superior performance in capturing high-resolution 3D leaf surfaces. With the development of robotic technologies, robot manipulators have been integrated into plant phenotyping systems (Chaudhury *et al.*, 2017; Gibbs *et al.*, 2018) to offer dexterity for sensor placement.

In order to understand the relationship between BR-mediated plant growth and drought responses, we developed a mobile robotic phenotyping system capable of (i) conducting time-course observations of plant growth using 2D and 3D imaging; (ii) administering the BR biosynthesis inhibitor Propiconazole (PCZ) to assess the BR response; and (iii) accurately controlling water levels for precise water deficit (drought) treatments. Our mobile robotic platform called Robotic Assay for Drought (RoAD) can automate daily weighing, watering, and non-destructive acquisition of 2D RGB images and high-precision 3D point clouds for BR and drought phenotyping experiments. Compared to existing phenotyping platforms, our system has significant improvements in mobility, sensor placement flexibility, and holographic imaging.

To make use of the data acquired by RoAD, we developed and validated algorithms for automated image processing, including rosette and individual leaf segmentation. Subsequent extraction of morphological traits and machine learning approaches allowed us to identify traits that distinguish

PCZ- or drought-treated plants from untreated controls. Using RoAD, we then examined BR and drought phenotypes of *Arabidopsis* mutants affected by BR signaling, diverse responses of 20 *Arabidopsis* accessions to PCZ treatment, and BR-mediated changes in the 3D architecture of maize (*Zea mays*) seedlings. Our results demonstrate that RoAD is a valuable tool to study BR-mediated control of plant growth and drought responses.

**RESULTS**

**Automated operation of RoAD: a Robotic Assay for Drought**

The RoAD system (Movie S1) was designed to perform non-destructive imaging, weighing, and watering. The images acquired provide valuable information for measuring the morphological traits of whole plants as well as individual leaves. The system is comprised of a custom-built mobile robot and two tables that can hold up to 240 pots

(Figure 1(a)). The robot was designed as an unmanned ground vehicle (UGV) (Shah *et al.*, 2016) carrying a Universal Robots UR10 manipulator (Universal Robots, Odense, Denmark) (Figure 1(b)). An RGB camera (exo249CU3, SVS-Vistek, Germany), a laser profilometer (LJ-V7300, Keyence, Japan), a gripper (2F-85, Robotiq Inc., Canada), and two water drippers are mounted to the end-effector of the manipulator. The camera position can be adjusted for plants of various heights. For example, *Arabidopsis* plants require a lower height than maize seedlings. The robot is equipped with a high-precision watering station that is composed of a bench scale (BSQ-0912-001, RMH Systems, United States) and two peristaltic pumps (DriveSure, Watson-Marlow, United Kingdom). Two kinds of liquid solutions can be administered to configure different watering regimes. The average absolute error of desired versus delivered water was 0.38 g (sample size: 26 078).

An experiment is initialized with a pot map, which stores the attributes of the plants, including plant genotype, the

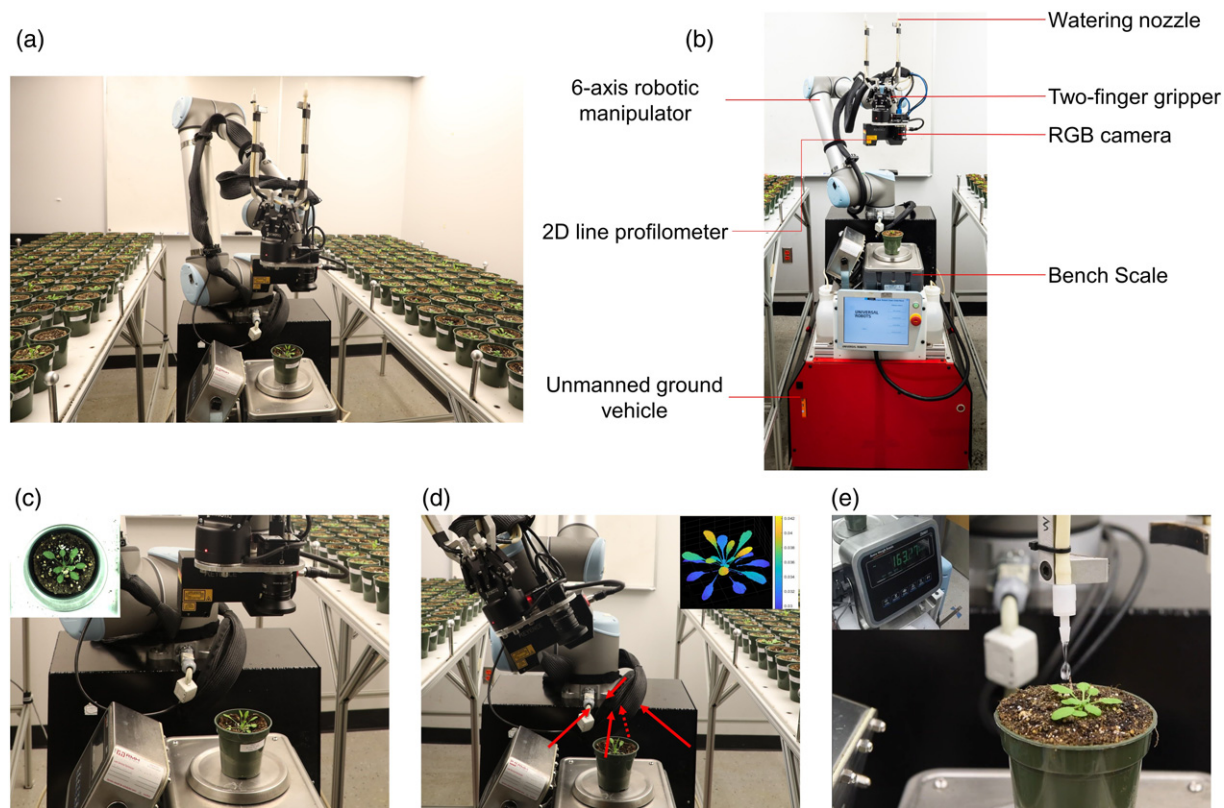


**Figure 1.** Overview of the RoAD system.

- (a) The RoAD system in action, with the mobile robot in between two tables that can each hold up to 240 10-cm-diameter pots.
- (b) The hardware setup of the RoAD system. Instruments for plant handling, imaging, and watering are mounted to a six-axis robotic manipulator. An RGB camera and a 2D line profilometer are used to acquire plant images. The two-finger gripper is used to pick up plants and place them on the bench scale. Watering nozzles attached to the gripper allow for water delivery from two separate water tanks.
- (c) RoAD collecting a top-view RGB image of a plant.
- (d) Multi-view scanning of a plant for the construction of 3D images. Four side-view images and one top-view image are acquired. Arrows indicate the direction of scanning.
- (e) Example of a plant being watered by the RoAD system. Plant weight is monitored by the bench scale in real-time to allow for precise control of water levels.

number of replicates, watering solution type, and target water level. Each day, the plants are imaged, weighed, and watered daily. During each data acquisition cycle, the robot parks at one of three positions adjacent to the plant tables. The manipulator is programmed to pick up each pot and place it on the scale. Image acquisition is performed before watering. First, a top-view RGB image is captured (Figure 1(c)). Then, the plant is scanned from five different perspectives by sweeping the laser profilometer around the plant (Figure 1(d)) for 3D reconstruction. Multiple scanning perspectives minimize occlusions in 3D reconstruction. The 3D surface model of the plant is reconstructed by cross-registering the 2D RGB image and the 3D point clouds. After image acquisition, the plant is then watered by one of the two peristaltic pumps to a predetermined soil moisture level (Figure 1(e)). Lastly, the pot is transported back to its position on the table. The aforementioned process takes approximately 1.5 min. Thus, the full cycle for 240 plants takes around 6 h, typically yielding 8 gigabytes of raw data (RGB images, 3D point cloud data, and pot weight data).

#### Automated processing of Arabidopsis plant images

Various strategies for analyzing image data and measuring growth phenotypes have been described (Minervini *et al.*, 2017; Zhou *et al.*, 2017), but general solutions for the segmentation of plants and individual leaves from 3D models are less developed (McCormick *et al.*, 2016). The RoAD system provides top-view 2D images of plants and multi-view 3D point clouds. To analyze the large amount of data generated by the RoAD system, we developed a fully automated image processing pipeline.

Our pipeline starts with plant segmentation of the RGB image, followed by segmentation of plants and leaves in the 3D point cloud. Based on the segmentation results, phenotypic trait values are extracted and saved as a CSV file for downstream analysis (Figure 2(a)). Plant segmentation in RGB images is based on color information (Figure 2(b)). Plant segmentation in 3D space starts with the points from the segmented RGB image projected onto 3D profiles. The resulting point cloud is then cleaned and analyzed to segment individual leaves. Previously developed methods for leaf segmentation have used 2D images, paired with deep learning methods that require large sets of data to achieve satisfactory performance (Chen *et al.*, 2019; Liu *et al.*, 2020). However, 2D-based leaf segmentation methods struggle when leaves overlap in images of a plant (such as the plants shown in Figure 2(b,c)), which tends to happen with increasing severity as plants progress through their growth cycle. The additional information gained by 3D images makes it easier to segment plant leaves.

The RoAD system provides a high-precision point cloud that facilitates image processing in 3D space. Based on the

superior 3D images, a surface-based segmentation (Figure 2(c)) was implemented to isolate the plant and individual leaves from the point cloud. The method is aimed at finding smoothly connected areas in point clouds using the constraints of local connectivity and surface smoothness (Rabbani *et al.*, 2006). The segmentation method consists of two steps: normal estimation and region growing. The surface normal and curvature (Rusu and Cousins, 2011) for each point are estimated by fitting a plane to the  $K$  nearest neighbors. The points of a typical Arabidopsis leaf should be locally connected to form a smooth surface with only minor variations between neighboring surface normals. Therefore, the process of region growing for one region starts with a seed point that has the minimum curvature. For the current seed, the algorithm finds its neighbors and checks the angle between the neighbor normal and the seed normal. The neighbor point is added to the current region if the angle is less than the threshold  $\theta_{th}$ . Among the neighbors, the points whose curvature is less than  $C_{th}$  are added to a queue of potential seed points. The current seed is removed from the queue and the process is repeated for the next available seed in the queue. The algorithm finishes growing the region until there are no seeds remaining in the queue. The one-region growing process is repeated for the rest of the unvisited points until all the points are segmented. The clusters that are sufficiently large and oriented towards the plant center are considered as leaf candidates. Based on trial and observation, we set the three thresholds  $K$ ,  $\theta_{th}$ , and  $C_{th}$  as 20,  $30^\circ$ , and 0.01, respectively.

#### Traits quantified by RoAD closely resemble ground truth measurements

The single-view point cloud can be incomplete because of leaf overlapping. To overcome this challenge, point clouds from multiple views were merged (Figure 2(c)). Here, we summarize the point-cloud processing pipeline, while a complete description of our algorithms is presented in the Experimental Procedures section. RoAD can provide holographic imaging of a plant, allowing a series of 3D traits such as plant height, plant volume, convex hull volume, leaf length, and leaf width to be extracted (Figure 2(d)). Plant volume is an important trait for estimating plant biomass. In this study, plant volume was calculated by first dividing the point cloud into horizontal slices with uniform thickness  $h$  ( $h = 2\text{ mm}$  for the experiments shown here). The volume of each slice was approximated by  $V_i = S_i \times h$ , where  $S_i$  is the horizontal projection area of the slice. The estimated volume was then calculated by summing the volume of all of the slices. Convex hull volume, which is a construct from computational geometry, provides a 3D measure of the volume of the space occupied by a plant. In addition, some secondary traits can be derived to describe the properties of plant architecture. For example, the plant



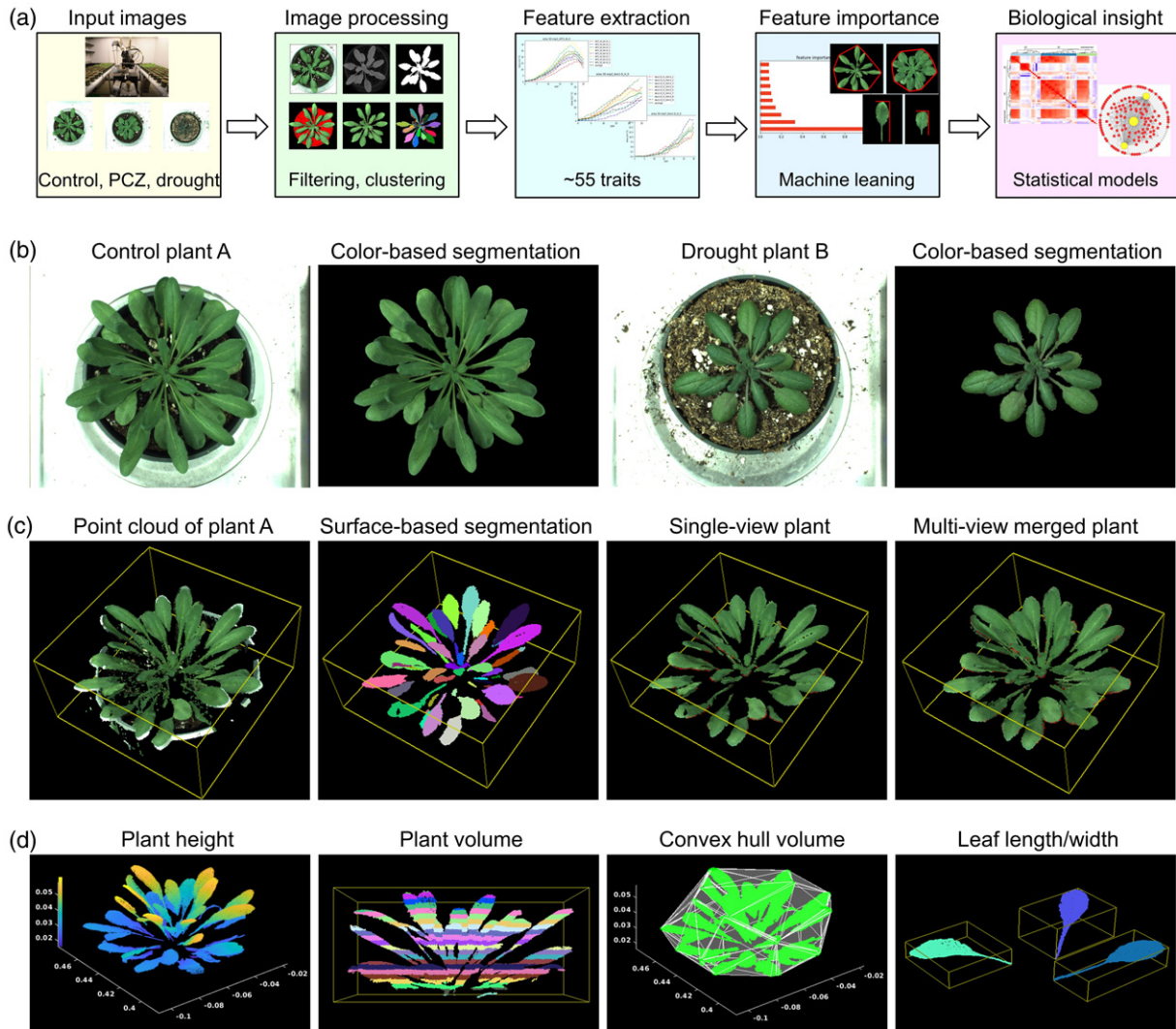


**Figure 2.** RoAD data analysis and phenotyping pipeline.

(a) Overview of RoAD system phenotyping and data analysis. 2D and 3D images are captured for plants under control, PCZ, and drought conditions. Image analysis is then performed for feature extraction. Fifty-five phenotypic traits calculated from the images are input variables for machine learning classifications. The most significant features were then used for biological analysis.

(b) Color-based plant segmentation in 2D. The excess green index was implemented to isolate a typical control plant. For drought-stressed plants, the pot position and the hue values in HSV color space were used as features for segmentation.

(c) Surface-based plant segmentation and registration in 3D. For each single-view point cloud, the segmented 2D plant is projected onto the 3D profile for removing the background, after which the surface-based segmentation is implemented to segment individual leaves based on surface smoothness and point connectivity. The segmented multi-view point clouds are aligned together to reconstruct full details of the plant.

(d) Typical 3D phenotypic traits generated by the image processing pipeline, including plant height, plant volume, convex hull volume, leaf length, and leaf width. The point cloud is sliced into multiple layers along the vertical direction to estimate the plant volume, where the volume of each slice is calculated by the multiplication of the horizontal area and the slice thickness. The ratio of plant volume to convex hull volume can be used to describe the plant compactness in 3D space.

compactness in 3D space can be quantified using 3D solidity, which is defined as the ratio of plant volume to convex hull volume.

An experiment at full capacity (240 plants) typically lasts 30 days and yields approximately 36 000 images. Phenotypic information related to plant growth, morphology, and color is obtained from the image data. These phenotypic traits can be categorized into four classes: color-related

traits, 2D holistic traits, 3D holistic traits, and individual leaf traits. Color-related traits can be an indicator of plant health (Klukas, 2014; Hüther *et al.*, 2020). Holistic level traits, such as plant area and plant volume, are obtained using measurements from the entire plant, while traits such as leaf width and leaf length are measured for individual leaves. In this study, the three largest leaves from each plant were selected to compute the individual leaf

traits. A total of 55 traits were extracted from the segmented images. As expected, we observed a high correlation between 2D, 3D, and individual leaf traits that act as proxies of plant growth (Figure 3(a)). For example, 3D convex area, 2D area, and individual leaf area were highly correlated. A full list of the extracted traits and the descriptions of how they were measured can be found in Table S1.

To evaluate the performance of the measurements obtained from the RoAD platform and image processing pipeline, 240 *Arabidopsis* plants under three different treatments were imaged. We also manually collected ground truth measurements of leaf length, leaf width, and fresh weight from the same set of plants. Comparisons between the system-derived traits and manual measurements indicated that RoAD accurately characterized phenotypic traits of interest (Figure 3(b, c)). For both leaf length and leaf width, the system-derived traits showed high R-squared values ( $R^2 > 0.96$ ) and aligned well with the diagonal reference line ( $x = y$ ), indicating that the RoAD platform can accurately measure leaf traits. We also compared plant volume with plant biomass measured as fresh weight, which showed a strong linear relationship (Figure 3(d)). Ultimately, the high R-squared values ( $R^2 > 0.95$ ) and low mean absolute errors demonstrate the utility of the RoAD platform for automated and reliable measurements of morphological traits.

### RoAD enables BR phenotyping in *Arabidopsis*

We used the RoAD system to measure growth phenotypes of four *Arabidopsis* genotypes, wild-type Col-0 (WT), *bri1-301*, *BRI1P-BRI1OX*, and *bes1-D*, under control or 100  $\mu\text{M}$  PCZ treatment conditions. The seeds of each genotype were germinated in Petri plates for 7 days and a single seedling was transferred to each pot. The plants were allowed to adapt to the soil for 2–3 days before the initiation of a RoAD experiment. During an experiment, each pot started with a well-watered condition. If the gravimetric water content fell below the target level (3 g water per g of soil), a specific amount of water or PCZ solution was added to maintain the pot at the desired condition. The 2D and 3D data were collected daily using the RoAD platform for 30 days, starting the first day after setup (DAS). The day when the system was set up was denoted by 0 DAS.

Given the large number of traits reported by the RoAD system, we first determined which of these traits are informative for the BR response. We used machine learning to classify WT plants between control and PCZ-treated categories. Our analysis attained test accuracies of up to 0.950 (Table S2) and identified a number of traits with high feature importance in distinguishing the BR-inhibited (PCZ-treated) plants from the controls (Figure 4(a)). For example, 2D solidity, which is defined as the ratio of area to convex hull area in 2D, can effectively separate the controls and

the PCZ-treated plants (Figure 4(b)). The solidity of the PCZ-treated plants was higher than that of the controls, indicating PCZ-treated plants show more compact growth. This pattern was also apparent for the holistic area convexity trait (Figure 4(c)), which is a measure of compactness in 3D, and the leaf aspect ratio (Figure 4(d)), which is a measure of individual leaf shape. PCZ-treated plants showed a higher degree of compactness in 3D models and they have shorter, wider leaves than those of the controls. These macroscopic phenotypic traits observed upon PCZ treatment are consistent with a reduction in cell elongation resulting from BR inhibition (Hartwig *et al.*, 2012; Sekimata *et al.*, 2002; Best *et al.*, 2014; Oh *et al.*, 2016).

If the reduced BR signaling is associated with the more compact growth as measured by increased solidity, then *bri1-301*, a loss-of-function BR receptor mutant (Xu *et al.*, 2008), would be expected to show a pattern similar to PCZ-treated plants. Indeed, we observed increased solidity of *bri1-301* compared to WT (Figure 4(e,f)). Moreover, solidity showed an opposite trend for *BRI1P-BRI1OX*, which has increased BR signaling (Friedrichsen *et al.*, 2000). However, another gain-of-function BR mutant, *bes1-D* (Yin *et al.*, 2002), did not show increased solidity values (Figure 4(f)). It is likely that the highly curved leaves of *bes1-D* reduced the rosette compactness due to feedback inhibition of some BR traits in *bes1-D*. Except for *bes1-D*, the order of the solidity of the other three genotypes is *bri1-301* > WT > *BRI1P-BRI1OX*, indicating that increased BR signaling generally reduces plant solidity. A complete list of phenotypic values and corresponding statistical analysis is provided (Tables S3 and S4).

To test how RoAD can be used to phenotype diverse *Arabidopsis* lines, we examined 20 *Arabidopsis* accessions from the 1001 Genomes collection (Alonso-Blanco *et al.*, 2016; Kawakatsu *et al.*, 2016) under control and PCZ treatment conditions (Figure 5(a), Tables S5 and S6). These lines were selected due to either an increased or a decreased response to another BR inhibitor, brassinazole (BRZ) (Asami *et al.*, 2000), when compared to Col-0. We observed concordance between the seedling and plant growth assays in a number of cases. For example, Petergof and Sij 1/96 were stunted in seedling BRZ assays, and similarly, they displayed a dwarf phenotype in plant growth assays (Figures 5(a) and S1(a–d)). Across all 20 lines, there was not a strong correlation between solidity in adult plants in response to PCZ and BRZ responses in seedlings (Figures 5(b) and S1(e)). BRZ and PCZ response assays in dark-grown seedlings were largely consistent (Figure S1(f)), indicating the differences are unlikely to be caused by the use of BRZ versus PCZ. This suggests that additional insight can be gained through BR phenotyping of multiple developmental stages and traits. Consistent with this idea, we found significant genotype-by-PCZ treatment interactions for 40 traits with 19 accessions having at

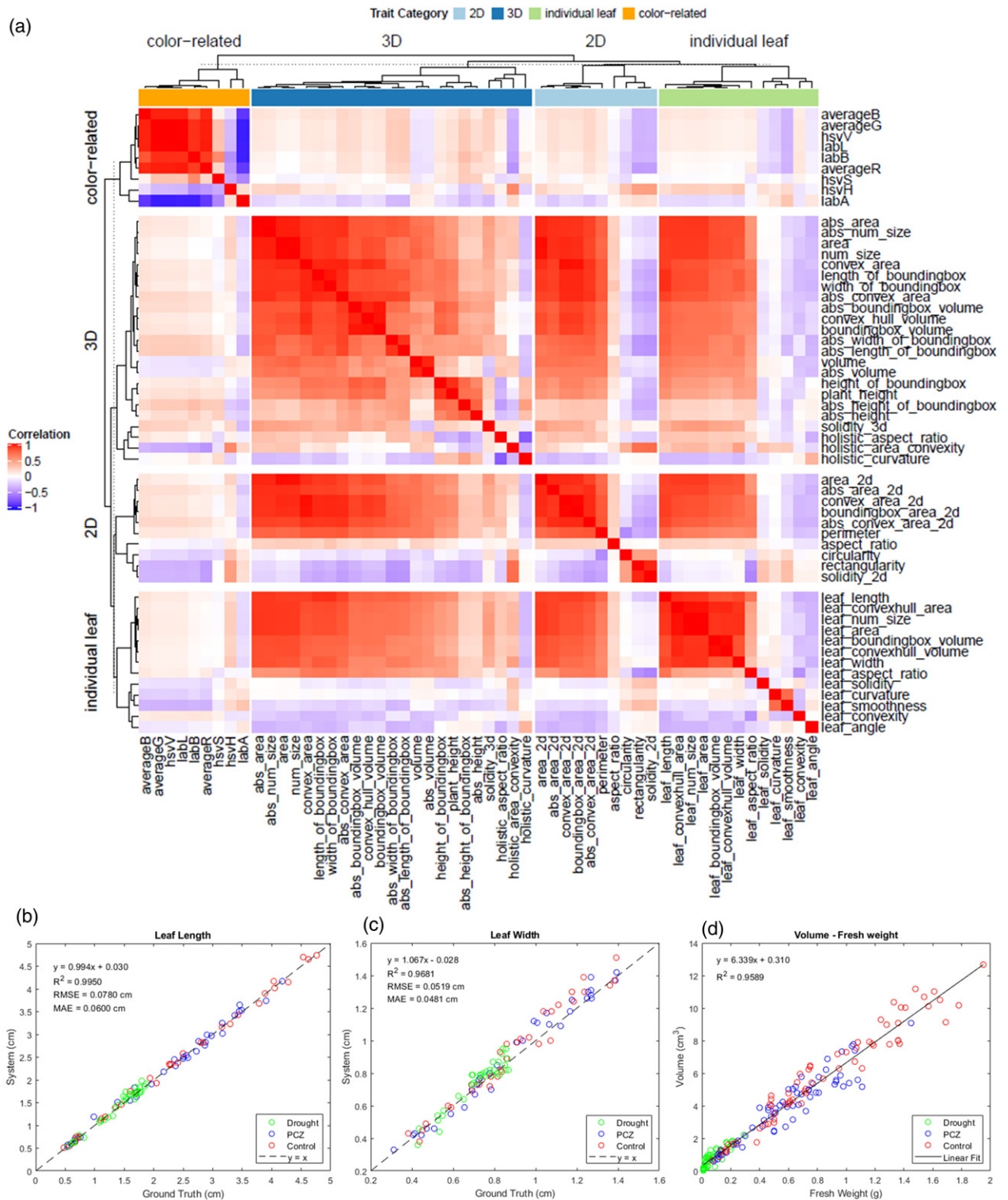


**Figure 3.** Correlation analysis of the image-derived traits of Arabidopsis plants. (a) Correlation among the 55 system-derived traits from RoAD image analysis. Traits are grouped by category and ordered by hierarchical clustering. (b) Correlation between system-derived traits and ground truth of data leaf length. (c) Correlation between system-derived traits and ground truth of data leaf width. (d) Correlation between system-derived plant volume and fresh weight.

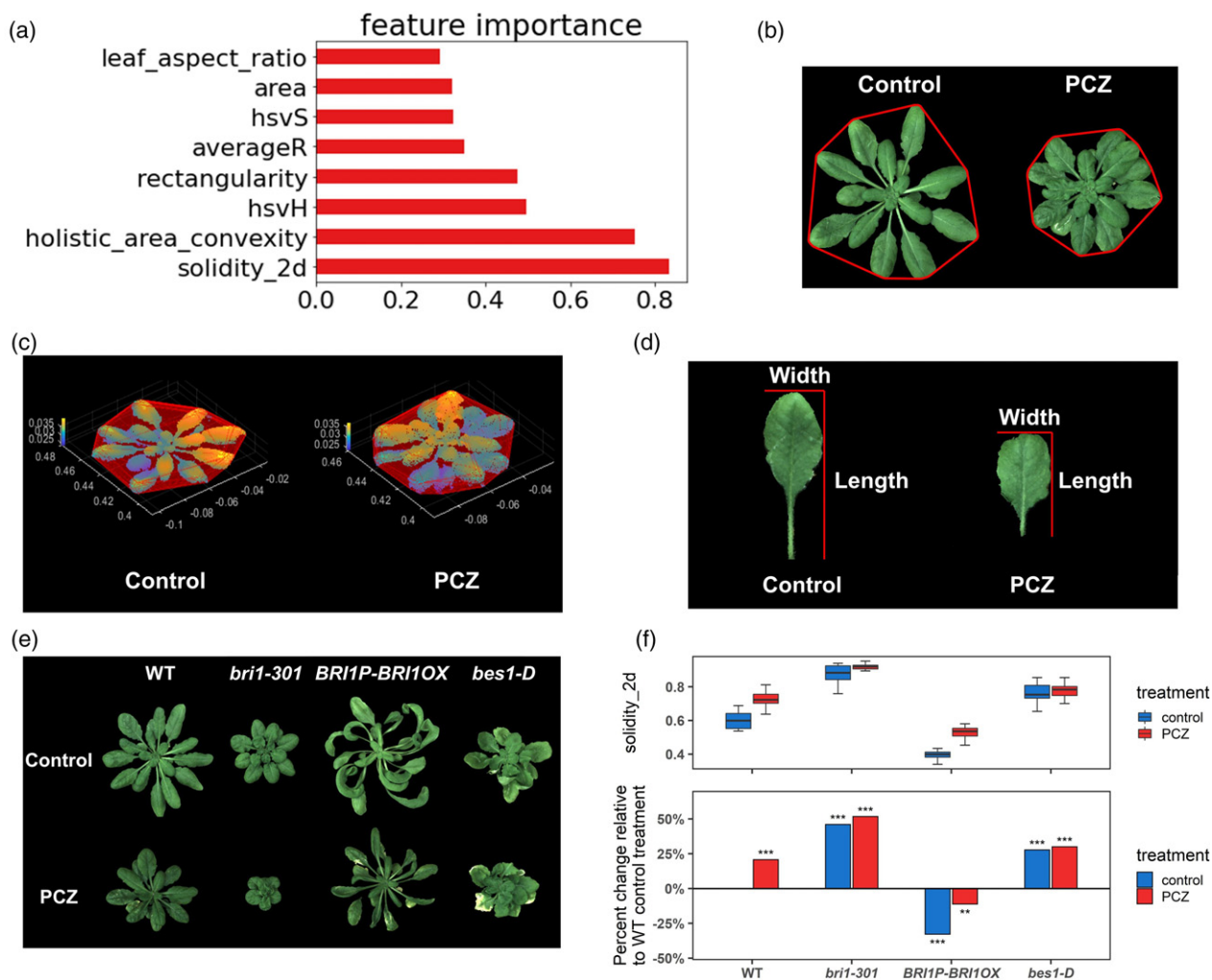


**Figure 4.** Patterns of BR phenotyping in Arabidopsis.

(a) Feature importance from machine learning classification of control versus PCZ-treated plants.

(b) Example of a 2D trait: solidity 2d, which is defined as the ratio of projected area to convex hull area. The red outline indicates the convex hull.

(c) Example of a 3D trait: holistic area convexity, defined as the ratio of plant area to the 3D convex hull area. Plants are pseudocolored based on the depth value and enclosed by a 3D convex hull.

(d) Example of an individual leaf trait: leaf aspect ratio, defined as the ratio of leaf length to leaf width.

(e) Representative images of WT, *bri1-301*, *BRI1P-BRI1OX*, and *bes1-D* plants under control or PCZ treatment (100  $\mu$ m) conditions at 30 days after setup (DAS).

(f) Solidity 2d of WT, *bri1-301*, *BRI1P-BRI1OX*, and *bes1-D* under control and PCZ treatment conditions at 30 DAS. FDR-corrected *P*-values relative to the WT control are indicated from the linear mixed model: +FDR < 0.1, \*FDR < 0.05, \*\*FDR < 0.01, \*\*\*FDR < 0.001.

least one significant difference (false discovery rate [FDR] < 0.1) when compared to the commonly used Col-0 accession (Figure 5(a,c)).

We noticed that the Lch-0 accession had a distinct 3D morphology and performed an additional experiment with Col-0 and Lch-0 under control, PCZ, and drought conditions (see next section for details on drought experiments). The 3D imaging capability of RoAD revealed that Lch-0 plants had increased plant height compared to Col-0 (Figure 6(a–d)) which coincided with longer hypocotyls in seedling BRZ assays (Figure S1(b,d)). We hypothesized that BRs may be at least partially responsible for the phenotypes observed in Lch-0. Consistent with this idea, Lch-0 had a significant

genotype-by-treatment interaction for plant height and convex hull volume under control versus PCZ treatment conditions (Figure 6(c–f)). Additionally, plant height and convex hull volume of Lch-0 also had a significant genotype-by-treatment interaction for drought (Figure 6(c–f)). This indicates that the 3D architecture of Lch-0 is influenced by both drought and BRs. The genotype-by-treatment interactions for Lch-0 were more subtle when only considering 2D traits such as convex area (Figure S1(g,h)). These results show that the RoAD system captures traits relevant to BR-regulated plant growth and drought responses, and can reveal additional plant characteristics that might be missed by phenotyping seedlings on Petri plates or by 2D images alone.



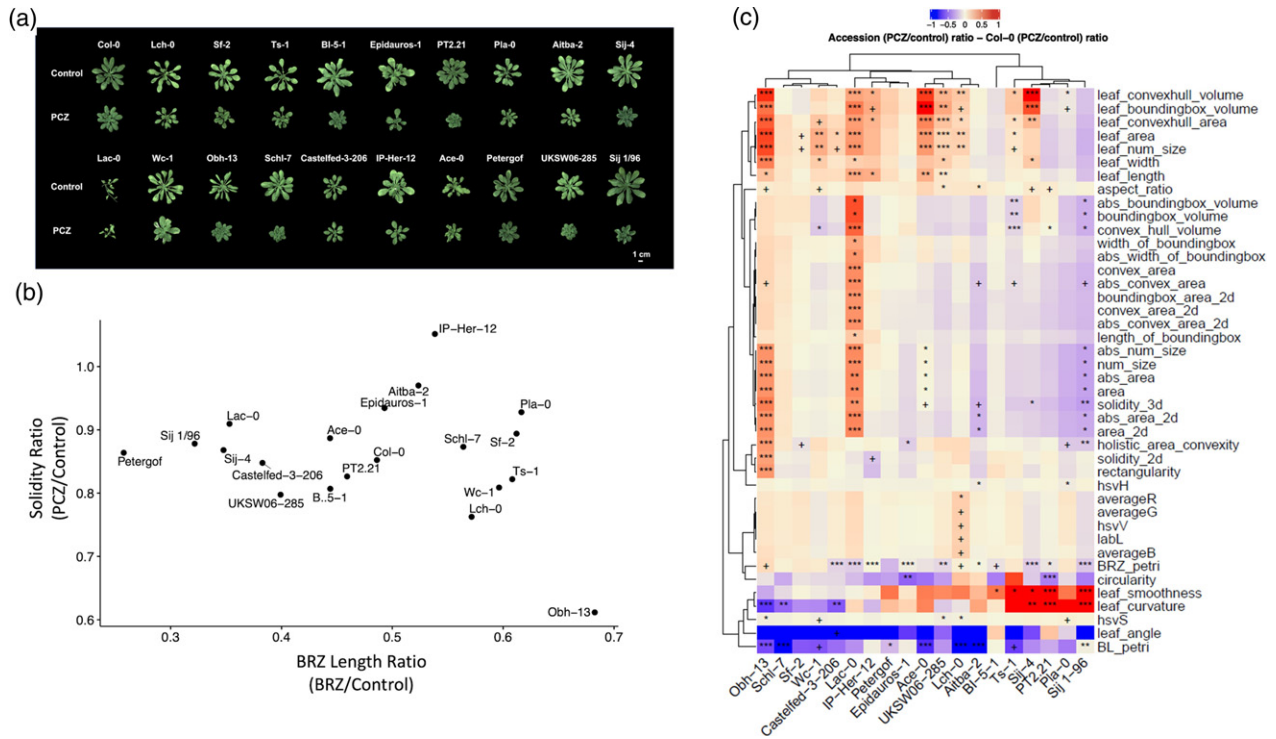


**Figure 5.** The PCZ response varies among Arabidopsis accessions. (a) Representative images of 20 Arabidopsis accessions grown under control or PCZ treatment (100  $\mu$ m) conditions taken at 29 DAS. (b) Comparison of solidity (PCZ/control ratio) from RoAD and the BRZ response in seedlings (BRZ/control length ratio) among the 20 accessions phenotyped. (c) Heatmap showing genotype-by-treatment effects for each accession compared to Col-0. BL\_petri indicates the response to 100 nM brassinolide in light-grown seedlings. BRZ\_petri indicates the response to 250 nM brassinazole in dark-grown seedlings. All other traits are from the PCZ response using RoAD at 29 DAS. FDR-corrected *P*-values are indicated for significant terms from a linear mixed model: +FDR < 0.1, \*FDR < 0.05, \*\*FDR < 0.01, \*\*\*FDR < 0.001.

### RoAD precisely controls water levels for drought experiments

The RoAD system can control soil water content for controlled drought experiments in two modes. The first is endpoint drought mode. In this type of experiment, the drought-stressed plants begin the experiment in well-watered conditions and are not watered until they fall below the target moisture level as assessed by gravimetric water content (Figure S2). One caveat of this method is that drying rates may vary among pots, which has been noted in other automated drought phenotyping systems (Tisné *et al.*, 2013). To address this issue, we implemented a second mode with controlled water deficit ramping. The plants under drought stress are kept in well-watered conditions for a set period (e.g., 8 days). Subsequently, the soil moisture level is decreased linearly, enabled by RoAD's daily weighing and watering regimen (Figure 7(a,b)). In this second mode, both the rate of drying and the timing of water deficit can be more precisely controlled.

To establish traits measured by RoAD that are informative for drought phenomics we implemented a similar machine learning classification on WT plants under control versus drought conditions (Table S2). From this analysis, we found that the trait hsvS, which refers to the average

saturation value in the HSV color space of the plant pixels, could efficiently distinguish control from drought-treated plants (Figure 7(c)). Specifically, drought-stressed plants had lower color saturation values than control plants.

We performed a controlled water deficit ramping drought experiment using WT, *bri1-301*, *BRI1P-BRI1OX*, and *bes1-D* in which water levels were reduced starting at 6 DAS (Drought 6), 8 DAS (Drought 8), or 10 DAS (Drought 10) (Figure 7(a,b), Tables S7 and S8). We first analyzed the color information but found that the genotypes responded similarly to drought in terms of color saturation (Figure 7(d)). Next, we examined growth responses in terms of plant area during the drought time series. We observed a more pronounced decrease in growth during drought conditions for both *bri1-301* and *bes1-D* compared to WT (Figures 6(f) and 7(e)). These results differ from water-withholding drought survival assays in which *bri1-301* plants have increased survival rates whereas *bes1-D* has decreased survival (Nolan *et al.*, 2017a; Ye *et al.*, 2017). While the conditions for traditional drought survival assays are more severe, the drought conditions applied from the RoAD system are milder, which might better represent field conditions. This suggests that monitoring growth during drought using the RoAD system could reveal additional aspects of BR-mediated growth and

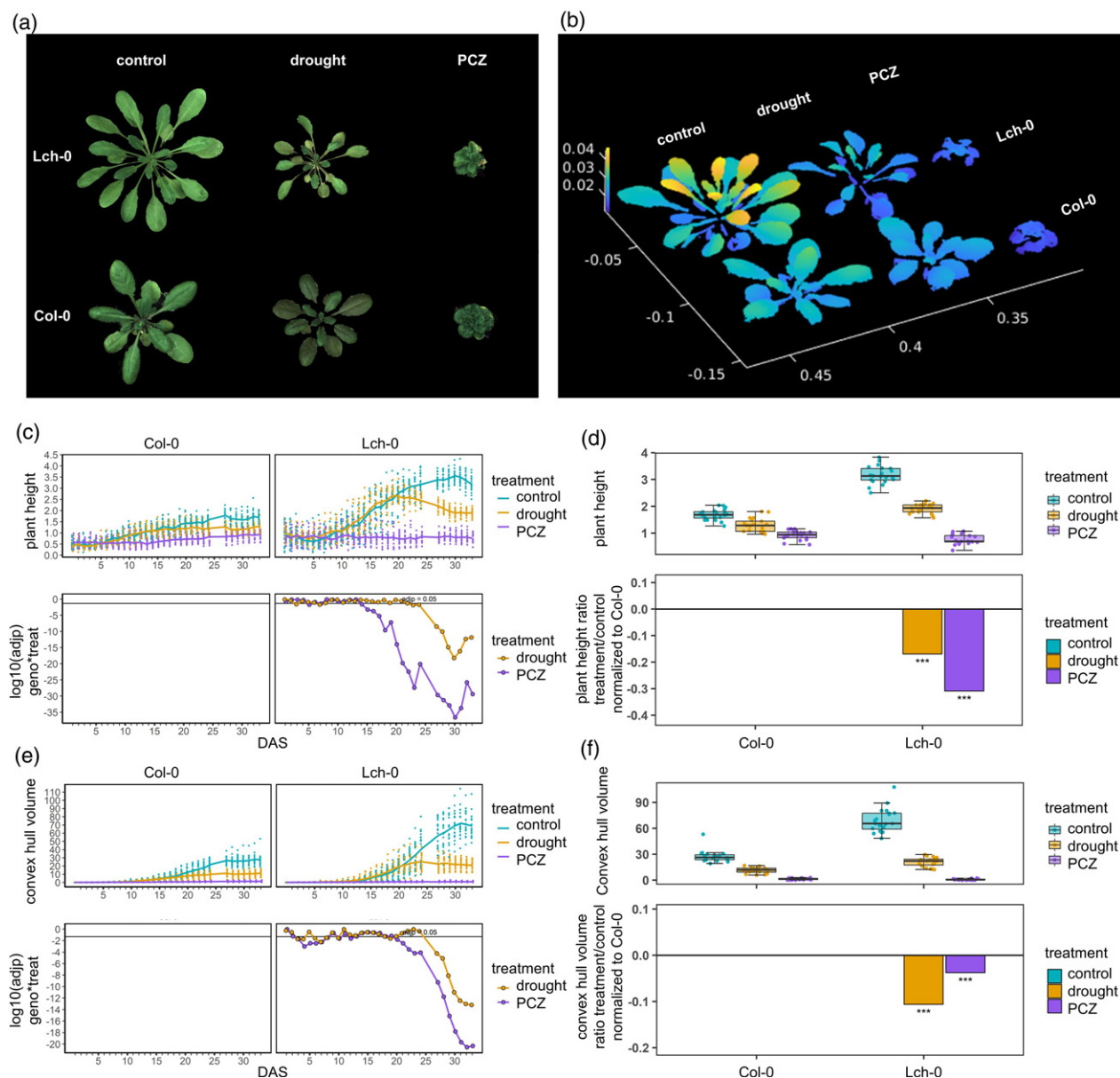


**Figure 6.** Lch-0 has an altered 3D architecture in response to PCZ and drought.

(a) Top-view images of representative plants of Col-0 and Lch-0 under control, drought, and PCZ conditions at 33 days after setup (DAS).

(b) Comparison of 3D models of representative plants of Col-0 and Lch-0 under control, drought, and PCZ conditions at 33 DAS.

(c) Plant height for Col-0 and Lch-0 under control, drought, and PCZ conditions.

(d) Comparison of plant height of Col-0 and Lch-0 under control, drought, and PCZ conditions at 33 DAS. FDR-corrected  $P$ -values are indicated for significant genotype-by-treatment interactions from a linear mixed model: +FDR < 0.1, \*FDR < 0.05, \*\*FDR < 0.01, \*\*\*FDR < 0.001.

(e) Convex hull volume for Col-0 and Lch-0 under control, drought, and PCZ conditions.

(f) Comparison of convex hull volume of Col-0 and Lch-0 under control, drought, and PCZ conditions at 33 DAS. FDR-corrected  $P$ -values are indicated for significant genotype-by-treatment interactions from a linear mixed model: +FDR < 0.1, \*FDR < 0.05, \*\*FDR < 0.01, \*\*\*FDR < 0.001.

stress coordination. Interestingly, the reduction of growth in *BRI1P-BRI1OX* plants under drought was less severe than that in WT plants (Figure 7(e,f)). This indicates that some aspects of the BR response that are increased in *BRI1P-BRI1OX* may help improve growth under drought. Taken together, the ability of the RoAD system to precisely control soil water conditions and monitor phenotypic traits should

prove instrumental in dissecting BR-mediated growth and drought responses.

### The 3D architecture of the BR response in maize seedlings is revealed by RoAD

To extend the RoAD system to row crops, we implemented RoAD assays in maize. PCZ has previously been

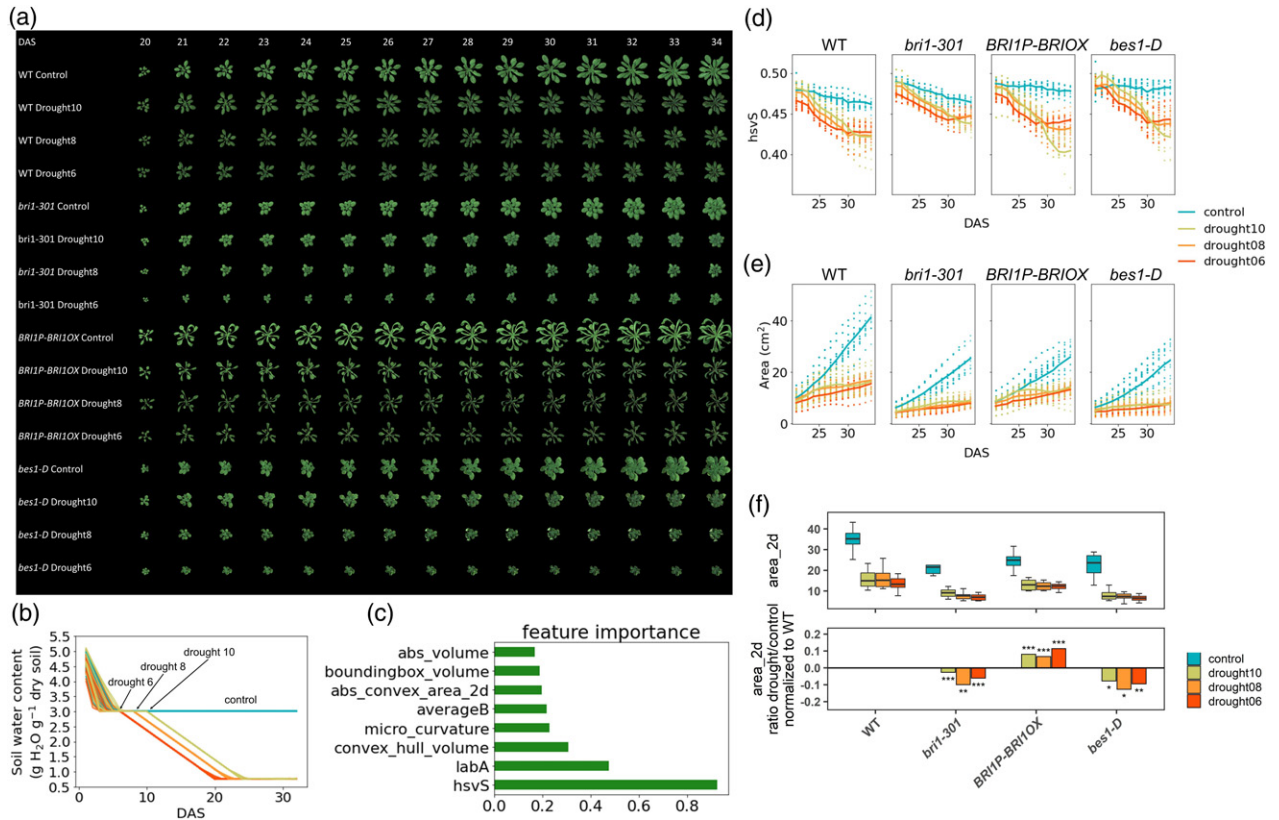


**Figure 7.** Drought responses in Arabidopsis. (a) Representative images of control and drought-treated WT, *bri1-301*, *bes1-D*, and *BRI1P-BRI1OX* plants from 20 to 34 days after setup (DAS). (b) Soil water content over time for control and drought-treated plants. For drought treatments the decrease in water levels was initiated at 6 DAS (Drought 6), 8 DAS (Drought 8), or 10 DAS (Drought 10) using controlled water deficit ramping. (c) Feature importance from machine learning classification of WT control and drought-treated plants. (d) Saturation (hsvS) values of WT, *bri1-301*, *BRI1P-BRI1OX*, and *bes1-D* plants under control and drought conditions. (e) Plant area for WT, *bri1-301*, *BRI1P-BRI1OX*, and *bes1-D* under control and drought conditions. Individual plant data are represented by dots, and the group averages are shown with solid lines. (f) Comparison of plant area of WT, *bri1-301*, *BRI1P-BRI1OX*, and *bes1-D* on 32 DAS. FDR-corrected *P*-values are indicated for significant genotype-by-drought interactions from a linear mixed model: +FDR < 0.1, \*FDR < 0.05, \*\*FDR < 0.01, \*\*\*FDR < 0.001.

demonstrated to be an effective BR inhibitor in maize, but the corresponding changes in 3D plant architecture have yet to be explored (Best *et al.*, 2017; Hartwig *et al.*, 2012). To this end, we developed a protocol for RoAD to carry out image acquisition for maize seedling plants non-destructively. During each acquisition cycle, a total of one RGB image and four multi-view point clouds were saved for each maize plant. The multi-view point clouds were filtered and then merged into a single point cloud (Figure 8 (a)). To compute the component phenotypes, a point cloud skeletonization method was used to analyze the maize plant architecture (Figure 8(b,c)) (Bao *et al.*, 2019a; Xiang *et al.*, 2019). A series of morphological traits were automatically extracted. Maize plants were grown in a growth chamber and imaged to evaluate the system and the image analysis algorithm. Comparisons between the measurements indicated that the RoAD platform provides accurate and reliable measurements for seedling maize plants (Figure S3, R<sup>2</sup> between 0.93 and 0.99).

Thirty maize plants with five levels of treatments (PCZ 0, 100 μM, 500 μM, 1000 μM, and 2000 μM) were grown to examine the effect of PCZ on maize seedling growth (Figure 8(d,e), Tables S9 and S10). Images were acquired daily from 10–14 days after planting (DAP). A set of phenotypic traits were extracted automatically using the developed algorithm. We plotted averaged growth curves by plant height, plant width, plant area, and plant volume per treatment (Figure S4(a–d)). PCZ inhibited growth of the maize plants, which was evident by the reduction of the plant height, plant width, plant area, and plant volume. These effects increased with the PCZ concentration. Consistent with our observations in Arabidopsis, the solidity for PCZ-treated maize plants was also increased compared with controls (Figure 8(f)). Next, we studied individual leaf traits to gain more detailed insights into the differences observed at the plant level. We found that the PCZ-treated plants had lower leaf curvature values than the control plants (Figure 8(g)). Leaf length also decreased for PCZ-

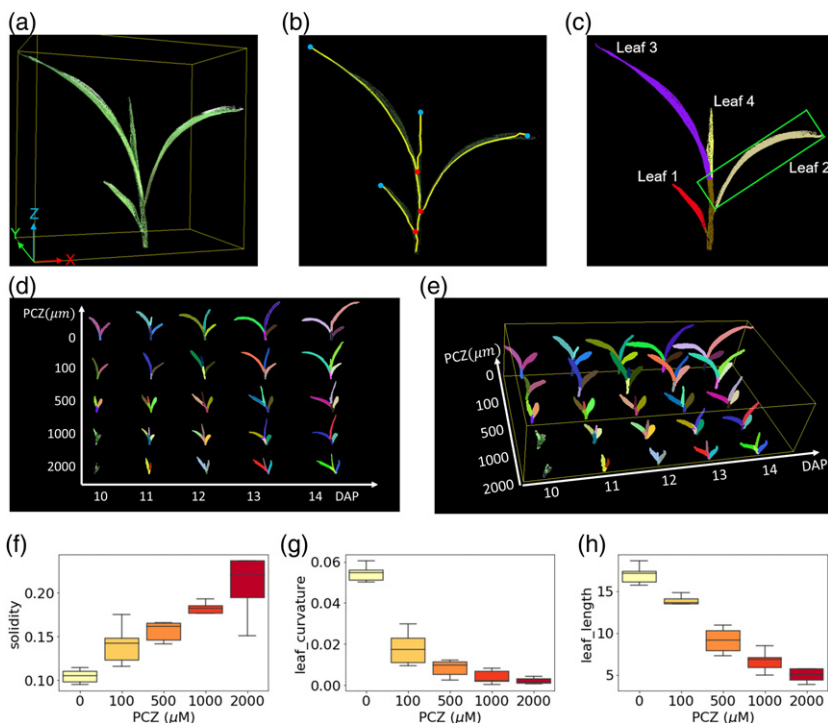


**Figure 8.** Image processing and BR phenotyping of maize seedlings.

(a) 3D point cloud of a maize plant.  
 (b) 3D skeleton of the plant. The blue and red points represent leaf tip and leaf base, respectively.  
 (c) Stem and leaf segmentation. The color indicates individually segmented leaves.  
 (d,e) Plant growth from 10 to 14 DAP shown in (d) 2D and (e) 3D view. Maize plants were divided into five groups and treated with 0, 100, 500, 1000, or 2000  $\mu\text{M}$  PCZ.  
 (f) Solidity of maize plants under different PCZ levels.  
 (g) Leaf curvature of the second leaf under the indicated control or PCZ treatment conditions.  
 (h) Leaf length of the second leaf under the indicated control or PCZ treatment conditions.

treated plants compared with the control plants (Figure 8 (h)). The decrease in leaf curvature and leaf length partially explained the increase in solidity observed and corroborated that PCZ treatment led to more compact maize seedling phenotypes. The trends observed in our phenotypic characterization of the maize seedling PCZ response are congruent with the described roles of BRs in controlling maize growth and development (Hartwig *et al.*, 2011; Hartwig *et al.*, 2012; Kir *et al.*, 2015) and provide insights into the 3D architecture of this response.

## DISCUSSION

In this study, we developed RoAD, an automated phenotyping system designed for analyzing BR and drought responses in *Arabidopsis*. The system is capable of watering and maintaining plants at different soil moisture conditions, as well as providing top-view RGB images and multi-view 3D point clouds of plants over time. RoAD incorporates an automatic image processing pipeline, supporting plant and leaf segmentation and calculation of morphological and color features. The pipeline was validated with manual measurements of plants. Overall, we found that the system-derived traits were highly correlated with the manually collected ground truth data. We assessed how traits measured by RoAD vary among BR mutants subjected to PCZ or drought conditions. Additionally, we phenotyped 20 *Arabidopsis* accessions under control and PCZ treatment conditions, which revealed substantial variation in

traits affected upon BR inhibition. The system was also used for maize seedling phenotyping, demonstrating that it is readily extensible to the analysis of other plant species.

The RoAD system differs from other previously developed phenotyping systems by (i) utilizing a mobile base, which can easily move to and fit in different growth chambers; (ii) adopting a six-axis robotic manipulator, making the robot more versatile, dexterous, and flexible to acquire multi-view images; and (iii) allowing multiple treatments such as PCZ and water limitation. In drought experiments, users can set when water limitation starts, the target water level, and when the target water level is reached. The robotic platform is extendable to other analytical sensors (such as near-infrared, thermal, and probing sensors) and could be integrated into facilities for large-scale plant phenotyping. A limitation of the RoAD system is that during each acquisition cycle, there is a gap of several hours between when the first and last plants of an experiment are processed, which means the timing of imaging and watering varies from plant to plant, but the data collection interval remains the same for every plant. To address the potential influence of the data acquisition timing difference, we have incorporated a randomized block design that avoids confounding between factors of interest such as genotypes or treatments and the acquisition order. It would be helpful to design multiple robots working in parallel to reduce the time between two data collections for different individuals.



Using RoAD and machine learning, we identified 2D solidity as an important feature in distinguishing control from PCZ-treated WT plants. While inhibition of the BR pathway by PCZ and a BR loss-of-function mutant, *bri1-301*, reduced plant solidity, increased BR signaling in *BRI1P-BRI1-OX* decreased solidity (Figure 4). On the other hand, *bes1-D*, which is also a BR gain-of-function mutant, had more complex phenotypes at the whole-plant level with increased solidity compared to WT Col-0. It is worth noting that the *bes1-D* mutant used in this study was introgressed into the Col-0 background (Vilarrasa-Blasi *et al.*, 2014), whereas this mutant was originally described in the Enkheim-2 (En2) background (Yin *et al.*, 2002). The increased solidity of the *bes1-D* allele used in this study might be due to highly curled leaves, likely due to feedback inhibition of the BR pathway.

By phenotyping 20 Arabidopsis accessions, we identified a large array of traits that responded to PCZ treatment differently than Col-0, which is often used as a WT control and reference accession (Figure 5). Additionally, the 3D imaging capabilities of RoAD detected altered plant height and convex hull volume in the Lch-0 accession, which would have been difficult to observe by 2D imaging (Figure 6). The plant height and convex hull volume of Lch-0 were significantly affected by PCZ and drought treatments compared to Col-0, indicating that both BRs and drought influence the 3D architecture and that this effect differs between Lch-0 and Col-0. The ability to capture 3D plant traits with RoAD will also be important when applying such a system to crop plants, such as maize. We noticed that seedling BR response assays did not always correlate with adult plant PCZ response phenotypes, suggesting complementarity among these assays. Our results demonstrate the utility of RoAD in phenotyping BR-mediated growth responses across different developmental stages, phenotypic traits, and genotypes.

BR and drought responses are extensively intertwined. Several mechanisms impinge on BES1 to balance BR-regulated growth responses with drought survival (Chen *et al.*, 2017; Nolan *et al.*, 2017a; Xie *et al.*, 2019; Ye *et al.*, 2017). Gain-of-function *bes1-D* mutants have reduced survival during drought, whereas loss-of-function *bri1-301* mutants display increased drought survival (Nolan *et al.*, 2017a; Ye *et al.*, 2017). Despite these opposite phenotypes in terms of drought survival, RoAD drought experiments showed that both *bes1-D* and *bri1-301* had more dramatic reductions in growth compared to WT under the drought conditions tested. On the other hand, the growth of BR gain-of-function *BRI1P-BRI1-OX* plants showed less inhibition in response to drought compared to WT. These phenotypes of *BRI1P-BRI1-OX* are interesting in light of the recent findings showing that overexpression of the vascular BR receptor *BRL3*, a homolog of *BRI1*, allows for increased drought survival without compromising plant growth (Fàbregas *et al.*, 2018; Planas-Riverola *et al.*, 2019).

Our findings suggest additional complexity in BR-mediated control of drought responses. Future studies should deconvolute the role of various BR signaling components in modulating both growth during drought and plant survival. The precise control of water levels and drought timing enabled by RoAD will enable such investigations.

In conclusion, the RoAD system provides a comprehensive and automated platform for BR and drought response experiments in soil-grown plants. The ability of RoAD to accurately measure morphological and growth-related traits of plants over time and under different treatments should prove a powerful resource to study the coordination between BR-mediated growth and stress responses.

## EXPERIMENTAL PROCEDURES

### Assembly of the RoAD system

RoAD consists of a mobile service robot and two elongated tables that support the pots. The robot is made up of an UGV (Shah *et al.*, 2016), a weighing station, a six-axis manipulator that carries an RGB camera, a laser profilometer, and an electric gripper with two liquid drippers at the fingertips. The robot is able to navigate in the growth chamber and pick up each pot on the tables with high reliability. The base of the UGV has a dimension of 73 cm × 73 cm × 51 cm. A T-slotted aluminum building system (80/20 Inc, United States) was used to build the frame of the vehicle. The UGV is equipped with four mecanum wheels (6" HD, AndyMark, United States) and magnetic guide sensors (MGS1600, Roboteq, United States). The mecanum wheels were driven by four brushless DC motors (BL58-412F-48V GRA60-032, Midwest Motion Products, United States) through two dual-channel motor controllers (FBL2360, Roboteq, United States). The motor controllers, the manipulator, and the sensors are controlled by an industrial-grade embedded computer (ML400G-30, Onlogic, United States). To reach all the pots on the tables, the UGV travels along a straight magnetic tape on the floor between the two tables. The UGV can autonomously move to three positions along the magnetic tape, which are enabled by the magnetic guide sensor and additional magnetic markers next to the magnetic tape. The two tables (71 cm × 213 cm) are made of rectangular plastic panels and 80/20 aluminum frames. As the magnetic guidance system has a position accuracy of ±1 cm, seven spherical metal balls of 2.54 cm in diameter are positioned along the edges of each table for the robot to accurately calibrate its pose with respect to the table. At each workstation, two balls on the near side of the table and one ball on the far side are scanned with the laser profilometer. Ball centers are estimated by fitting spheres to the resultant 3D point clouds. Subsequently, the pot positions in a grid system can be located with an accuracy of ±5 mm, which is determined by the accuracies of the hand-eye calibration, the synchronization between the laser profilometer and the manipulator, and sphere fitting. The space between adjacent pots on the table allows an approximately 1 cm tolerance. The 3D ball-based pose calibration method is essential to the high reliability of the RoAD platform.

A Graphic User Interface (GUI) was developed to set plant attributes, manage RoAD parameters, and control the RoAD system. To start a new experiment, the user needs to define plant attributes including plant genotype, the number of replicates, watering solution type and target water level. Subsequently, a pot map is generated using a randomized complete block design. In the pot map, each plant has a unique ID. The GUI allows the user to

set the drought mode and tune parameters such as the exposure time of the RGB camera, the vertical distance from the camera to the plant, and the speed and acceleration of the robotic manipulator. The user can select various operation modes based on the needs of the experiment. In mode 1, RoAD will grab pots given by the user and put them on the table sequentially. Mode 2 is for daily image acquisition and watering of the plants on the tables. Mode 3 is designed to image and scan a plant that is manually placed on the bench scale.

### Plant materials and growth conditions

Our experiments on the RoAD system included the following *Arabidopsis thaliana* (*Arabidopsis*) lines: WT Col-0, *bes1-D* (Vilarrasa-Blasi *et al.*, 2014; Yin *et al.*, 2002), *BRI1P-BRI1OX* (Friedrichsen *et al.*, 2000), *bri1-301* (Xu *et al.*, 2008), and the 20 *Arabidopsis* accession listed in Table S11. Plants were grown under control (3 g water per g dry soil), PCZ (3 g water with 100  $\mu\text{M}$  PCZ added per g dry soil) (Hartwig *et al.*, 2012; Sekimata *et al.*, 2002; Best *et al.*, 2014; Oh *et al.*, 2016), or drought conditions (0.75 g water per g dry soil). Plant seeds were sown on  $\frac{1}{2}$  Linsmair and Skoog plates supplemented with 1% sucrose and stratified at 4°C in darkness for 2–5 days. Plates were then placed in the light at 22°C. After 7 days, the plants were transferred to 10-cm-diameter pots filled with equal weights of soil, and soaked in plastic trays with water or PCZ solution. The exact mass of dry soil was determined for each experiment, so that the gravimetric water content could be calculated to reach the desired soil moisture level. Plants were positioned on the two tables using a randomized complete block design with four to eight replications per genotype per treatment. Lighting in the growth room was set to a 12/12-h light/dark cycle. A dehumidifier was used to maintain the relative humidity at approximately 50%. Weighing and watering were performed once a day for each pot, according to the target conditions. The plants were imaged for approximately 30 days, starting from the day when the plants were placed in the phenotyping system. For trait validation, the leaf length and width were measured manually using the MATLAB image processing toolbox and converted from units of pixels to centimeters using a pinhole camera model.

For the BRZ response experiments, we sterilized seeds for 4 h in a Nalgene Acrylic Desiccator Cabinet (Fisher Scientific, 08-642-22) by mixing 200 mL bleach (8.25% sodium hypochlorite) with 8 mL concentrated hydrochloric acid to generate chlorine gas. Seeds were then resuspended using 0.1% agarose solution for plating. Control (BRZ0; DMSO solvent only) or BRZ-treated (250 nM) 1/2 LS plates were supplemented with 1% (w/v) sucrose. After seeds were plated, the plates were sealed with breathable tape (3M Micropore) and placed in the dark at 4°C for 5 days. Plates were then exposed to light for 6–8 h and wrapped in foil for 7 days of growth in the dark. Plates were imaged with an Epson Perfection V600 Flatbed Photo Scanner at a resolution of 1200 dots per inch and hypocotyls were then measured in ImageJ.

Brassinolide (BL) response experiments were carried out in a similar fashion, except that plates were supplemented with control solvent (BL0, DMSO) or 100 nM BL (Wako chemicals) and plants were grown for 7 days at 22°C under continuous light.

To compare BRZ and PCZ treatments in seedlings, we selected 250 nM PCZ and 500 nM BRZ as concentrations that resulted in a similar decrease in hypocotyl elongation for WT Col-0. BRZ and PCZ response assays were then performed side-by-side using 7-day old seedlings that were grown in the dark using the methods described above for BRZ assays.

Maize plants were studied to further extend the application of the RoAD system to crop plants. B73 maize seeds were planted in

plastic pots in a growth chamber, with one seed per pot. The plants were divided into five experimental groups and one control group. The plants in the experimental groups were watered with indicated concentrations of PCZ (100  $\mu\text{M}$ , 500  $\mu\text{M}$ , 1000  $\mu\text{M}$ , or 2000  $\mu\text{M}$ ), and the plants in the control group were grown with water. The plants were cultivated in a growth chamber (16 h light/8 h dark) at a temperature of 28°C and a relative humidity of 50%. Thirty individual plants were randomly selected from all six groups, with five replicates in each group to be inspected by the RoAD system. Image acquisition was performed at five different developmental time points (once a day from 10 to 14 DAP). One RGB image and four multi-view depth images were acquired for each plant. The maize plants were manually transported from the growth chamber to the RoAD system.

### Image processing

**Segmentation of *Arabidopsis* plants in 2D.** The excess green (ExG) index has been found to be an effective indicator to separate green plants from soil (Hamuda *et al.*, 2016). In our pipeline, the RGB image is first converted to a grayscale image using the ExG index and then binarized by Otsu's thresholding method (Figure 2(b)). However, we observed that the plants under water-limited conditions tend to exhibit a dark purple color at late growth stages (Figures 7(a) and S2(a)). Accordingly, we implemented hue information in HSV (hue, saturation, and value) color space to identify the dark purple parts. The pot edges were detected using Circle Hough Transform to aid in the isolation of plants. The part inside the detected circle was considered the region of interest (ROI). The ROI was then transformed to HSV color space. An appropriate threshold was then applied to the hue channel of the ROI to separate the drought plant from the soil. The mask images from ExG and HSV color space were combined to acquire a plant-only RGB image. The 2D image processing pipeline was implemented in MATLAB R2017a (MathWorks, United States).

**Segmentation and registration of *Arabidopsis* plants in 3D.** The 3D point cloud processing pipeline utilized the Point Cloud Library (Rusu and Cousins, 2011) and the OpenCV library (Bradski and Kaehler, 2008). First, the point cloud was down-sampled and filtered to reserve only the parts that were common among the multi-view point clouds (plant, soil, and pot). We then implemented the iterative closest point algorithm to find the global transformation between multiple point clouds taken from different viewing angles. At this stage, four transformation matrices were obtained, which were used to merge the point clouds. In the next step, we segmented the plant canopy by mapping the foreground from the 2D image to the point cloud. The resulting point cloud was filtered and cleaned by removing small clusters. After that, the segmented plants from each frame were merged into a single frame, using the transformation matrices obtained in the registration process. Finally, in order to remove the duplicate points without losing important information, a voxel grid filter with a 3D box size of 5 mm<sup>3</sup> was applied to the combined point cloud.

**Maize plant image analysis and trait validation.** A point cloud skeletonization method was introduced to analyze the maize plant architecture and segment individual leaves. The raw data (Figure S5(a)) were filtered and merged to a single point cloud (Figure S5(b)). To compute the plant height, the random sample consensus algorithm (Fischler and Bolles, 1981) was implemented to fit a plane in the merged point cloud to detect the soil (Figure S5(c)). The points were sliced into layers based on their height

and Euclidean clusters were extracted for grouping each layer. The 3D skeleton was generated and mapped to a graph by connecting the centroid of the adjacent Euclidean clusters (Figure S5(d)). The individual leaf was detected by iteratively traversing the graph from a one-neighbor node (leaf tip, blue points) along a connected path until encountering a three-neighbor node (leaf base, red points) (Figure S5(e)). Leaves were numbered consecutively, with the first leaf being closest to the soil. The stem was detected as a 3D Hough line (Figure S5(f)). Based on the segmentation results, a series of morphological traits were automatically extracted (Table S1).

A total of 21 maize plants were grown in a growth chamber and studied to evaluate the system and the proposed algorithm. The plants were sampled at 20 days after planting. The position of the camera was adjusted based on the heights of the plants. After image acquisition, plants were manually measured to collect ground truth data. Plant height and plant width were measured using a ruler. Subsequently, each leaf was cut off to measure the leaf length and leaf area. Leaf length was measured as the distance from leaf base to tip. The leaf was then scanned using an Epson Perfection V600 Flatbed Photo Scanner and quantified using MATLAB to obtain the area.

### Linear mixed model analysis

A linear mixed-effects model was fit to the trait data using the lme function in the R nlme package (Pinheiro *et al.*, 2020). For each trait and day, the mixed model used raw trait measurements as the dependent variable with fixed effects of genotype, treatment, and their interaction. The random effects structure consisted of a random intercept of plant index within block. Genotype-specific weights were assigned to account for unequal variance across genotypes. The model specification was as follows:  $\text{lme}(\text{raw value} \sim \text{genotype} * \text{treatment}, \text{random} = 1|\text{block}/\text{index}, \text{weights} = \text{var}(\text{form} = \sim 1|\text{geno}))$ . For all plotted data, *P*-values were adjusted for multiple testing according to (Benjamini and Hochberg, 1995).

### Machine learning classification

To understand the underlying relationship between system-derived phenotypic traits and plant responses to PCZ or drought treatments, we constructed two-class classification models based on four supervised machine learning methods: a least absolute shrinkage and selection operator (LASSO) (Tibshirani, 1996), a support vector machine (SVM) (Smola and Schölkopf, 2004), a random forest (Breiman, 2001), and Adaptive Boosting (AdaBoost) (Hastie *et al.*, 2009). LASSO is a parametric method that is capable of addressing collinearity issues in high-dimensional feature selection setups (Li *et al.*, 2019). The idea of LASSO is to add a penalty term into parameter estimation and shrink the least important feature's coefficient to zero. We used the LASSO estimator integrated with logistic regression for classification (Moghimi *et al.*, 2018). SVM is one of the most robust prediction methods, and it constructs a hyperplane with soft margins for classification. The linear kernel function was used for the SVM classifier in this study in order to get the feature weight. The non-parametric method from machine learning provides an alternative solution to avoid the problems caused by multicollinearity among variables (Tomaschek *et al.*, 2018). Both random forest and AdaBoost are non-parametric models that make predictions based on a number of decision trees, while the former uses bagging and the latter uses adaptive boosting as the ensemble method. Random forest aggregates hundreds of de-correlated decision trees trained on a randomly selected bootstrapped dataset. On the other hand, AdaBoost trains decision trees in a sequential way by increasing the weight of data points misclassified by previous classifiers.

The classifications with labeling '1' for control and '2' for PCZ were performed for WT Arabidopsis plants with DAS values larger than 15. The full dataset of WT plant morphological traits under control and PCZ conditions was shuffled and split into two groups with 70% for training and 30% for testing with 10-fold cross-validation. Feature importance was calculated for each model to assess the relative contribution of each trait in the classification process, and the averaged feature importance ranking was obtained from the four models. The mean and standard deviation of accuracy, F1, precision, and recall values of the four classifiers are reported in Table S2. The same processing pipeline was applied to WT plants with DAS values larger than 24 to classify control and drought-stressed Arabidopsis plants. Machine learning classification methods were implemented in Python 2.7.14 (Python Software Foundation, United States) using scikit-image v0.13.0 (Pedregosa *et al.*, 2011).

### ACKNOWLEDGMENTS

This work was supported by funding from the Plant Sciences Institute (PSI) at Iowa State University and the National Science Foundation (MCB 1818160 to YY and JWW) and by Postdoctoral Research Fellowships in Biology Program (IOS-2010686 to TMN). We thank Patrick Schnable, Dan Nettleton, Natalie Clark, and Hongqing Guo for helpful suggestions, Hao Jiang and Le Wang for technical assistance, and Eugenia Russinova for BRI1P-BRI1-OX seeds.

### AUTHOR CONTRIBUTIONS

Conceptualization, TMN, LX, YY, LT, and SHH. Methodology, LX, YB, ME, and TMN. Software, LX and YB. Investigation, TMN, ME, LX, PW, NMH, AMH, and SAM. Resources, YB, TT, JG, DS, and LX. Data curation, LX, TMN, and ME. Visualization, LX, TMN, and ME. Writing – original draft, LX, TMN, ME, and YY. Writing – review & editing, LX, TMN, ME, YY, YB, LT, SHH, and JWW. Funding acquisition, YY, LT, JWW, and SHH.

### CONFLICTS OF INTEREST

The authors declare no conflict of interest.

### DATA AVAILABILITY STATEMENT

All relevant data can be found within the manuscript and its supporting materials. The source code for Arabidopsis image processing is available on GitHub at <https://github.com/lr-xiang/RoAD-image-processing>.

### SUPPORTING INFORMATION

Additional Supporting Information may be found in the online version of this article.

**Figure S1.** PCZ and BRZ responses of Arabidopsis accessions.

**Figure S2.** Drought responses in Arabidopsis using RoAD endpoint drought mode.

**Figure S3.** Validation results for maize plants.

**Figure S4.** Comparison of traits extracted from 3D point cloud of maize plants.

**Figure S5.** Processing of image data to segment maize seedling stems and leaves.

**Table S1.** Description of morphological traits extracted from Arabidopsis and maize images.

**Table S2.** Machine learning performance metrics from control vs. PCZ and control vs. drought classification.

**Table S3.** Phenotypic traits from PCZ response experiments using WT, *bri1-301*, *BRI1P-BRI1-OX*, and *bes1-D* Arabidopsis plants.

**Table S4.** Linear mixed model statistical analysis of the PCZ response using WT, *bri1-301*, *BRI1P-BRI1-OX*, and *bes1-D* Arabidopsis plants.

**Table S5.** Phenotypic traits from PCZ response experiments using 20 Arabidopsis accessions.

**Table S6.** Linear mixed model statistical analysis from PCZ response experiments using 20 Arabidopsis accessions.

**Table S7.** Phenotypic traits from drought response experiments using WT, *bri1-301*, *BRI1P-BRI1-OX*, and *bes1-D* Arabidopsis plants.

**Table S8.** Linear mixed model statistical analysis of the drought response using WT, *bri1-301*, *BRI1P-BRI1-OX*, and *bes1-D* Arabidopsis plants.

**Table S9.** Plant traits from maize PCZ phenotyping experiments.

**Table S10.** Individual leaf traits from maize PCZ phenotyping experiments.

**Table S11.** Description and stock numbers of 20 Arabidopsis accessions used in this study.

**Movie S1.** Video showing RoAD in motion.

## REFERENCES

- Alonso-Blanco, C., Andrade, J., Becker, C., Bemm, F., Bergelson, J., Borgwardt, K.M. et al. (2016) 1,135 Genomes reveal the global pattern of polymorphism in Arabidopsis thaliana. *Cell*, **166**, 481–491.
- An, N., Welch, S.M., Markelz, R.J.C., Baker, R.L., Palmer, C.M., Ta, J. et al. (2017) Quantifying time-series of leaf morphology using 2D and 3D photogrammetry methods for high-throughput plant phenotyping. *Computer Electronics in Agriculture*, **135**, 222–232.
- Apelt, F., Breuer, D., Nikoloski, Z., Stitt, M. & Kragler, F. (2015) Phytotyping<sup>4D</sup>: a light-field imaging system for non-invasive and accurate monitoring of spatio-temporal plant growth. *The Plant Journal*, **82**, 693–706.
- Asami, T., Min, Y.K., Nagata, N., Yamagishi, K., Takatsuto, S., Fujioka, S. et al. (2000) Characterization of brassinazole, a triazole-type brassinosteroid biosynthesis inhibitor. *Plant Physiology*, **123**, 93–99.
- Bao, Y., Tang, L., Srinivasan, S. & Schnable, P.S. (2019a) Field-based architectural traits characterisation of maize plant using time-of-flight 3D imaging. *Biosystems Engineering*, **178**, 86–101.
- Bao, Y., Zarecor, S., Shah, D., Tuel, T., Campbell, D.A., Chapman, A.V.E. et al. (2019b) Assessing plant performance in the Envratron. *Plant Methods*, **15**, 117.
- Behmann, J., Acebron, K., Emin, D., Bennertz, S., Matsubara, S., Thomas, S. et al. (2018) Specim IQ: Evaluation of a new, miniaturized handheld hyperspectral camera and its application for plant phenotyping and disease detection. *Sensors (Switzerland)*, **18**(2), 441.
- Benjamini, Y. & Hochberg, Y. (1995) Controlling the false discovery rate: a practical and powerful approach to multiple testing. *Journal of the Royal Statistical Society. Series B*, **57**, 289–300.
- Bernotas, G., Scorza, L.C.T., Hansen, M.F., Hales, I.J., Halliday, K.J., Smith, L.N. et al. (2019) A photometric stereo-based 3D imaging system using computer vision and deep learning for tracking plant growth. *Giga-science*, **8**, 1–15.
- Best, N.B., Hartwig, T., Budka, J.S., Bishop, B.J., Brown, E., Potluri, D.P.V. et al. (2014) Soilless Plant Growth Media Influence the Efficacy of Phytohormones and Phytohormone Bennett, I.M. (Ed.). *PLoS One*, **9**, e107689.
- Best, N.B., Johal, G. & Dilkes, B.P. (2017) Phytohormone inhibitor treatments phenocopy brassinosteroid-gibberellin dwarf mutant interactions in maize. *Plant Direct*, **1**(2). <https://doi.org/10.1002/pld3.9>.
- Bradski, G.R. & Kaehler, A. (2008) *Learning OpenCV: computer vision with the OpenCV library* 1st edition. O'Reilly.
- Breiman, L. (2001) Random forests. *Machine Learning*, **45**, 5–32.
- Chaudhury, A., Ward, C., Talasaz, A., Ivanov, A.G., Brophy, M., Grodzinski, B. et al. (2017) Machine vision system for 3D plant phenotyping. *ArXiv*, **16**, 2009–2022.
- Chen, D., Neumann, K., Friedel, S., Kilian, B., Chen, M., Altmann, T. et al. (2014) Dissecting the phenotypic components of crop plant growth and drought responses based on high-throughput image. *Analysis*, **26**, 4636–4655.
- Chen, J., Nolan, T.M., Ye, H., Zhang, M., Tong, H., Xin, P. et al. (2017) Arabidopsis WRKY46, WRKY54, and WRKY70 transcription factors are involved in brassinosteroid-regulated plant growth and drought responses. *The Plant Cell*, **29**, 1425–1439.
- Chen, Y., Baireddy, S., Cai, E., Yang, C. & Delp, E.J. (2019) Leaf segmentation by functional modeling. In *Proceedings of the IEEE/CVF Conference on Computer Vision and Pattern Recognition Workshops* (pp. 0–0).
- Clauw, P., Coppens, F., Beuf, K.D., Dhondt, S., Daele, T.V., Maleux, K., et al. (2015) Leaf Responses to Mild Drought Stress in Natural Variants of Arabidopsis. *Plant Physiology*, **167**(3), 800–816.
- Clouse, S.D., Langford, M. & McMorris, T.C. (1996) A Brassinosteroid-Insensitive mutant in Arabidopsis thaliana exhibits multiple defects in growth and development. *Plant Physiology*, **111**, 671–678.
- Dubois, M. & Inzé, D. (2020) Plant growth under suboptimal water conditions: early responses and methods to study them. *Journal of Experimental Botany*, **71**, 1706–1722.
- Fàbregas, N., Lozano-Elena, F., Blasco-Escámez, D., Tohge, T., Martínez-Andújar, C., Albacete, A. et al. (2018) Overexpression of the vascular brassinosteroid receptor BRL3 confers drought resistance without penalizing plant growth. *Nature Communications*, **9**, 1–13.
- Fischler, M.A. & Bolles, R.C. (1981) Random sample consensus: a paradigm for model fitting with applications to image analysis and automated cartography. *Communications of the ACM*, **24**, 381–395.
- Friedrichsen, D.M., Joazeiro, C.A.P., Li, J., Hunter, T. & Chory, J. (2000) Brassinosteroid-insensitive-1 is a ubiquitously expressed leucine-rich repeat receptor serine/threonine kinase. *Plant Physiology*, **123**, 1247–1255.
- Fujita, M., Tanabata, T., Urano, K., Kikuchi, S. & Shinozaki, K. (2018) RIPPS: a plant phenotyping system for quantitative evaluation of growth under controlled environmental stress conditions. *Plant and Cell Physiology*, **59**, 2030–2038.
- Ge, Y., Bai, G., Stoerger, V. & Schnable, J.C. (2016) Temporal dynamics of maize plant growth, water use, and leaf water content using automated high throughput RGB and hyperspectral imaging. *Computers and Electronics in Agriculture*, **127**, 625–632.
- Gibbs, J.A., Pound, M., French, A.P., Wells, D.M., Murchie, E. & Pridmore, T. (2018) Plant phenotyping: an active vision cell for three-dimensional plant shoot reconstruction. *Plant Physiology*, **178**, 524–534.
- Granier, C., Aguirrezabal, L., Chenu, K., Cookson, S.J., Dauzat, M. Hamard, P. et al. (2006) PHENOPSIS, an automated platform for reproducible phenotyping of plant responses to soil water deficit in *Arabidopsis thaliana* permitted the identification of an accession with low sensitivity to soil water deficit. *New Phytologist*, **169**, 623–635.
- Gupta, A., Rico-Medina, A. & Caño-Delgado, A.I. (2020). The physiology of plant responses to drought. *Science* (80-.). **368**:266–269.
- Hamuda, E., Glavin, M. & Jones, E. (2016) A survey of image processing techniques for plant extraction and segmentation in the field. *Computers and Electronics in Agriculture*, **125**, 184–199.
- Hartwig, T., Chuck, G.S., Fujioka, S., Klempien, A., Weizbauer, R., Potluri, D.P.V. et al. (2011) Brassinosteroid control of sex determination in maize. *Proceedings of the National Academy of Sciences of the United States of America*, **108**, 19814–19819.
- Hartwig, T., Corvalan, C., Best, N.B., Budka, J.S., Zhu, J.-Y., Choe, S. et al. (2012) Propiconazole Is a Specific and Accessible Brassinosteroid (BR) Biosynthesis Inhibitor for Arabidopsis and Maize. *PLoS One*, **7**, e36625.
- Hastie, T., Rosset, S., Zhu, J. & Zou, H. (2009) Multi-class AdaBoost. *Stat Interface*, **2**, 349–360.
- Hu, Y., Wang, L.e., Xiang, L., Wu, Q. & Jiang, H. (2018) Automatic non-destructive growth measurement of leafy vegetables based on Kinect. *Sensors*, **18**, 806.
- Hüther, P., Schandry, N., Jandrasits, K., Bezrukov, I. & Becker, C. (2020) ARA-DEEOPSIS, an automated workflow for top-view plant phenomics using semantic segmentation of leaf States. *The Plant Cell*, **32**, 3674–3688.
- Kaminuma, E., Heida, N., Tsumoto, Y., Yamamoto, N., Goto, N., Okamoto, N. et al. (2004) Automatic quantification of morphological traits via three-dimensional measurement of Arabidopsis. *The Plant Journal*, **38**, 358–365.
- Kawakatsu, T., Huang, S.-S., Jupe, F., Sasaki, E., Schmitz, R.J., Urich, M.A. et al. (2016) Epigenomic diversity in a global collection of Arabidopsis thaliana accessions. *Cell*, **166**, 492–505.



- Kir, G., Ye, H., Nelissen, H., Neelakandan, A.K., Kusnandar, A.S., Luo, A. *et al.* (2015) RNA interference knockdown of BRASSINOSTEROID INSENSITIVE1 in maize reveals novel functions for brassinosteroid signaling in controlling plant architecture. *Plant Physiology*, **169**, 826–839.
- Klem, K., Mishra, K.B., Novotná, K., Rapantová, B., Hodaňová, P., Mishra, A. *et al.* (2017) Distinct growth and physiological responses of Arabidopsis thaliana natural accessions to drought stress and their detection using spectral reflectance and thermal imaging. *Functional Plant Biology*, **44**, 312.
- Li, J., Nagpal, P., Vitart, V., McMorris, T.C. & Chory, J. (1996). A role for brassinosteroids in light-dependent development of Arabidopsis. *Science (80- )*, **272**:398–401.
- Li, J., Veeranampalayam-Sivakumar, A.-N., Bhatta, M., Garst, N.D., Stoll, H., Stephen Baenziger, P. *et al.* (2019) Principal variable selection to explain grain yield variation in winter wheat from features extracted from UAV imagery. *Plant Methods*, **15**, 1–13.
- Liu, D., Zhang, D., Song, Y., Huang, H. & Cai, W. (2020) Panoptic feature fusion net: a novel instance segmentation paradigm for biomedical and biological images. *IEEE Transactions on Image Processing*, **30**, 2045–2059.
- Mccormick, R.F., Truong, S.K. & Mullet, J.E. (2016) 3D sorghum reconstructions from depth images identify QTL regulating shoot architecture. *Plant Physiology*, **172**:pp.00948.2016.
- Minervini, M., Abdelsamea, M.M. & Tsafaris, S.A. (2014) Image-based plant phenotyping with incremental learning and active contours. *Ecological Informatics*, **23**, 35–48.
- Minervini, M., Giuffrida, M.V., Perata, P. & Tsafaris, S.A. (2017) Phenotiki: an open software and hardware platform for affordable and easy image-based phenotyping of rosette-shaped plants. *The Plant Journal*, **90**, 204–216.
- Moghim, A., Yang, C. & Marchetto, P.M. (2018) Ensemble feature selection for plant phenotyping: a journey from hyperspectral to multispectral imaging. *IEEE Access*, **6**, 56870–56884.
- Neumann, K., Klukas, C., Friedel, S., Rischbeck, P., Chen, D., Entzian, A. *et al.* (2015) Dissecting spatiotemporal biomass accumulation in barley under different water regimes using high-throughput image analysis. *Plant, Cell and Environment*, **38**, 1980–1996.
- Nolan, T.M., Brennan, B., Yang, M., Chen, J., Zhang, M., Li, Z. *et al.* (2017a) Selective autophagy of BES1 mediated by DSK2 balances plant growth and survival. *Developmental Cell*, **41**, 33–46.e7.
- Nolan, T.M., Chen, J. & Yin, Y. (2017b) Cross-talk of Brassinosteroid signaling in controlling growth and stress responses. *The Biochemical Journal*, **474**, 2641–2661.
- Nolan, T.M., Vukašinić, N., Liu, D., Russinova, E. & Yin, Y. (2020) Brassinosteroids: Multidimensional regulators of plant growth, development, and stress responses. *The Plant Cell*, **32**(2), 295–318.
- Northey, J.G.B., Liang, S., Jamshed, M., Deb, S., Foo, E., Reid, J.B. *et al.* (2016) Farnesylation mediates brassinosteroid biosynthesis to regulate abscisic acid responses. *Nature Plants*, **2**(8), 1–7. <https://doi.org/10.1038/nplants.2016.114>.
- Oh, K., Matsumoto, T., Hoshi, T. & Yoshizawa, Y. (2016) *In vitro* and *in vivo* evidence for the inhibition of brassinosteroid synthesis by propiconazole through interference with side chain hydroxylation. *Plant Signaling & Behavior*, **11**, e1158372.
- Pedregosa, F., Varoquaux, G., Gramfort, A., Michel, V., Thirion, B., Grisel, O. *et al.* (2011) Scikit-learn: machine learning in Python. *The Journal of Machine Learning Research*, **12**, 2825–2830.
- Pinheiro, J., Bates, D., DebRoy, S. & Sarkar, D.; Team, R.C. (2020) nlme: Linear and Nonlinear Mixed Effects Models version 3.1-147 from CRAN.
- Planas-Riverola, A., Gupta, A., Betegoñ-Putze, I., Bosch, N., Iban s, M. & Cano-Delgado, A.I. (2019) Brassinosteroid signaling in plant development and adaptation to stress. *Development*, **146**(5). <https://doi.org/10.1242/dev.151894>.
- Rabbani, T., Van Den Heuvel, F. & Vosselmann, G. (2006) Segmentation of point clouds using smoothness constraint. *International archives of photogrammetry, remote sensing and spatial information sciences*, **36**(5), 248–253.
- Rousseau, C., Belin, E., Bove, E., Rousseau, D., Fabre, F., Berruyer, R. *et al.* (2013) High throughput quantitative phenotyping of plant resistance using chlorophyll fluorescence image analysis. *Plant Methods*, **9**, 17.
- Rusu, R.B. & Cousins, S. (2011) 3D is here: Point Cloud Library (PCL). In *2011 IEEE International Conference on Robotics and Automation*, pp. 1–4. IEEE
- Sekimata, K., Han, S.Y., Yoneyama, K., Takeuchi, Y., Yoshida, S. & Asami, T. (2002) A specific and potent inhibitor of brassinosteroid biosynthesis possessing a dioxolane ring. *Journal of Agriculture and Food Chemistry*, **50**, 3486–3490.
- Shah, D., Tang, L., Gai, J. & Putta-Venkata, R. (2016) Development of a mobile robotic phenotyping system for growth chamber-based studies of genotype x environment interactions. *IFAC-PapersOnLine*, **49**, 248–253.
- Skiryicz, A., Vandenbroucke, K., Clauw, P., Maleux, K., De Meyer, B., Dhondt, S. *et al.* (2011) Survival and growth of Arabidopsis plants given limited water are not equal. *Nature Biotechnology*, **29**, 212–214.
- Smola, A.J. & Schölkopf, B. (2004) A tutorial on support vector regression. *Statistics and computing*, **14**, 199–222.
- Sun, Y., Fan, X.Y., Cao, D.M., Tang, W., He, K., Zhu, J.Y. *et al.* (2010) Integration of Brassinosteroid signal transduction with the transcription network for plant growth regulation in Arabidopsis. *Developmental Cell*, **19**, 765–777.
- Szekeres, M., Németh, K., Koncz-Kálmán, Z., Mathur, J., Kauschmann, A., Altmann, T. *et al.* (1996) Brassinosteroids rescue the deficiency of CYP90, a cytochrome P450, controlling cell elongation and de-etiolation in Arabidopsis. *Cell*, **85**, 171–182.
- Tibshirani, R. (1996) Regression shrinkage and selection via the lasso. *Journal of the Royal Statistical Society: Series B*, **58**, 267–288.
- Tisné, S., Serrand, Y., Bach, L., Gilbault, E., Ben Ameer, R., Balasse, H. *et al.* (2013) Phenoscope: an automated large-scale phenotyping platform offering high spatial homogeneity. *The Plant Journal*, **74**, 534–544.
- Tomaschek, F., Hendrix, P. & Baayen, R.H. (2018) Strategies for addressing collinearity in multivariate linguistic data. *Journal of Phonetics*, **71**, 249–267.
- Van Dooren, T.J.M., Silveira, A.B., Gilbault, E., Jiménez-Gómez, J.M., Martin, A., Bach, L. *et al.* (2020) Mild drought in the vegetative stage induces phenotypic, gene expression, and DNA methylation plasticity in Arabidopsis but no transgenerational effects. *Journal of Experimental Botany*, **71**(12), 3588–3602.
- Vilarrasa-Blasi, J., González-García, M.P., Frigola, D., Fàbregas, N., Alexiou, K.G., López-Bigas, N. *et al.* (2014) Regulation of plant stem cell quiescence by a brassinosteroid signaling module. *Developmental Cell*, **30**, 36–47.
- Xiang, L., Bao, Y., Tang, L., Ortiz, D. & Salas-Fernandez, M.G. (2019) Automated morphological traits extraction for sorghum plants via 3D point cloud data analysis. *Computers and Electronics in Agriculture*, **162**, 951–961.
- Xie, Z., Nolan, T., Jiang, H., Tang, B., Zhang, M., Li, Z. *et al.* (2019) The AP2/ERF transcription factor TINY modulates brassinosteroid-regulated plant growth and drought responses in Arabidopsis. *The Plant Cell*, **31**, 1788–1806.
- Xu, W., Huang, J., Li, B., Li, J. & Wang, Y. (2008) Is kinase activity essential for biological functions of BRI1? *Cell Research*, **18**, 472–478.
- Yao, J., Sun, D., Cen, H., Xu, H., Weng, H., Yuan, F. *et al.* (2018) Phenotyping of Arabidopsis drought stress response using kinetic chlorophyll fluorescence and multicolor fluorescence. *Imaging*, **9**, 1–15.
- Ye, H., Liu, S., Tang, B., Chen, J., Xie, Z., Nolan, T.M. *et al.* (2017) RD26 mediates crosstalk between drought and brassinosteroid signalling pathways. *Nature Communications*, **8**(1), <https://doi.org/10.1038/ncomms14573>.
- Yin, Y., Wang, Z.Y., Mora-García, S., Li, J., Yoshida, S., Asami, T. *et al.* (2002) BES1 accumulates in the nucleus in response to brassinosteroids to regulate gene expression and promote stem elongation. *Cell*, **109**, 181–191.
- Yu, X., Li, L., Zola, J., Aluru, M., Ye, H., Foudree, A. *et al.* (2011) A brassinosteroid transcriptional network revealed by genome-wide identification of BES1 target genes in Arabidopsis thaliana. *The Plant Journal*, **65**, 634–646.
- Zhou, J., Applegate, C., Alonso, A.D., Reynolds, D., Orford, S., Mackiewicz, M. *et al.* (2017) Leaf-GP: An open and automated software application for measuring growth phenotypes for Arabidopsis and wheat. *Plant Methods*, **13**, 117.
- Zia, S., Romano, G., Spreer, W., Sanchez, C., Cairns, J., Araus, J.L. *et al.* (2013) Infrared thermal imaging as a rapid tool for identifying water-stress tolerant maize genotypes of different phenology. *Journal of Agronomy and Crop Science*, **199**, 75–84.